Quantum entanglement creation for distant quantum memories via time-bin multiplexing

Zhihao Xie,[1] Yijie Liu,[1] Xiang Mo,[1] Tao Li,[1,2,*] and Zhenhua Li[1,2]
[1]*School of Science, Nanjing University of Science and Technology, Nanjing 210094, China*
[2]*MIIT Key Laboratory of Semiconductor Microstructure, Nanjing University of Science and Technology, Nanjing 210094, China*

(Received 23 August 2021; revised 10 November 2021; accepted 23 November 2021; published 6 December 2021)

Quantum networks require parallel quantum entanglement between pairs of distant quantum memories (QMs) for practical applications. However, usually one pair of QMs is entangled using a single photonic pulse and multiple pulses are consumed to generate parallel entanglement between pairs of QMs. We propose a multiplexing method for simultaneously entangling multiple pairs of QMs located in two distant nodes. A single photon with high-dimensional encoding first entangles with all QMs in one node, leading to hybrid entanglement between a high-dimensional photon and two-dimensional QMs, and then it interacts with QMs in the other node and converts the hybrid entanglement to entanglement between multiple pairs of QMs in a heralded way. This can significantly increase the efficiency of large-scale quantum networks by reducing the exponential transmission loss via time-bin multiplexing. Furthermore, this protocol presents a specific connection between high-dimensional and two-dimensional quantum systems.

DOI: 10.1103/PhysRevA.104.062409

I. INTRODUCTION

Quantum entanglement plays an essential part in various quantum technologies and enables practical applications that significantly overwhelm their classical counterparts [1–5]. Especially, nonlocal quantum entanglement between two distant nodes is of central importance in large-scale quantum communication [6–10] and distributed quantum computation [11–14]. The propagation of photonic pulses is a prerequisite for the generation of nonlocal quantum entanglement [15,16], however, the transmission loss of optical fibers or free-space channels always increases exponentially with the transmission distance [17], which sets a limit on the efficiency and the range of entanglement generation between two distant nodes. The quantum repeater [18–21] provides a polynomial speedup of the generation of an entangled channel by dividing it into several intermediate segments and generating entanglement parallelly in each one, in combination with quantum swapping [22–25] and quantum purification [26–29].

In general, there are two main approaches to generate entanglement over a channel with an intermediate range [30,31]: One generates hybrid entanglement between a photonic pulse and an individual stationary qubit [e.g., quantum memory (QM)] [32–35] and sends the pulse to interact with another QM [36–42]; and the other generates one hybrid entangled state at each node and interferes the two pulses at an intermediate node [43–48]. Obviously, the generation of entanglement between a pair of remote QMs requires the effective transmission of a photonic pulse between two nodes. Recently, quantum multiplexing [42] for generation of two pairs of QMs was proposed and analyzed in detail by exploring the hyperencoding qubits of a single photon in both the polarization and the time-bin degrees of freedom (DoFs). Furthermore, this approach could be generalized to entangle more pairs of QMs by encoding more DoFs of a photon [49].

In contrast to qubits hyperencoded in multiple DoFs of a photon [49], the qudit with more than two states has been studied intensively because of its remarkable properties, such as the higher information-carrying capacity, the increased resistance to noise, the enhancement of the algorithm efficiency, and the advantage for a fundamental test of nature [50–52]. For single photons, there are various DoFs with high dimensions that can be used to encode qudits. The path or momentum, transverse spatial modes, and time bins inherently involve many quantum states and have been explored for implementing different quantum techniques [53–58]. Especially, the time-bin qudit of a photon is perfectly suited for transmission over large distances using either free-space channels or fibers [59]. A high-dimensional quantum key distribution (QKD) over tens of kilometers has been demonstrated using Franson-type interference [60,61] and the noise resistance of time-bin entanglement distribution has been demonstrated in an 80-dimension space [62].

Solid-state spin systems (e.g., color centers in diamond) are convenient structures with excellent optical properties and are a promising candidate for the realization of quantum repeater networks [63–66]. In 2006, Childress *et al.* proposed a fault-tolerant protocol for quantum entanglement generation in nitrogen-vacancy (NV) color centers in diamond [67]. The entanglement between a pair of electron spins was generated after the interference of two optical modes followed by a projective measurement. Subsequently, state-dependent scattering of single photons by an NV color center coupled to an optical cavity was used to entangle electron spins [68–71]. Furthermore, the state-dependent scattering approach has also been used to construct universal quantum

*tao.li@njust.edu.cn

gates on electron spins and photons [72–76] and to generate cluster states for one-way quantum computation [77–79]. Recently, Piparo *et al.* showed that a memory-assisted QKD with NV centers outperforms a memoryless one [80,81]. Moreover, a single silicon vacancy (SiV) center integrated inside a diamond nanophotonic cavity has been demonstrated to be an efficient interface between single photons and individual spins, enabling asynchronous photonic Bell-state measurement and photon-mediated interactions between two SiV centers [82–84]. Furthermore, some interesting protocols with color centers have been studied for various quantum technologies [85–87].

In this article, we propose a multiplexing protocol for generating entanglement between distant QMs. Entanglement of multiple pairs of QMs can be simultaneously achieved in a heralded way by using the auxiliary time-bin qudit of a polarized single photon rather than multiple DoFs or independent photons. The outline of our protocol in principle is identical to that of the original entanglement generation protocol [36–42]. Specifically, after the interaction between the high-dimensional encoded single photon with all QMs in one node, the photon and QMs are evolved into a hybrid entangled state [88,89], in which a proper measurement on the photon can predict the state of all QMs. The photon acts as a data bus connecting two nodes and then converts the hybrid entangled state into a product state of multiple Bell states of QM pairs. Therefore, our protocol can generate entanglement between multiple QM pairs in a heralded way by the transmission and measurement of a single photon and reduces the influence of both the transmission loss and the finite single-photon measurement efficiency on entanglement generation. Moreover, quantum multiplexing photons each carrying multiple qubits may reduce the resource requirement for distributed quantum information processing tasks [90], in which transmission loss is the dominant source of error. These features, combined with spatial-mode multiplexing [91], enable higher entangling rates and multiple pairs of entangled QMs, and then can enhance fully connected multinode quantum networks [92,93]. Meanwhile, our protocol provides a method to study the conversion and connection between high-dimensional quantum systems and two-dimensional ones.

The paper is organized as follows: A quantum interface between a single photon and an individual color center is introduced briefly in Sec. II. An entanglement generation protocol for three pairs of QMs is presented in Sec. III. Subsequently, in Sec. IV, a generalized protocol for generating ($n > 3$) pairs of QMs is described. In Sec. V, the performance of entanglement creation is presented. Finally, we conclude with a brief discussion and summary in Sec. VI.

II. AN EFFECTIVE SINGLE-PHOTON AND INDIVIDUAL SPIN INTERFACE BASED ON COLOR-CENTER COUPLING TO AN OPTICAL CAVITY

An interface between single photons and individual spins, enabling hybrid entanglement between them, is an essential building block for quantum networks and distributed quantum computation [30,38]. A deterministic spin-photon interface can be achieved by a color center that is coupled to a single-sided cavity, shown in Fig. 1. A negatively charged

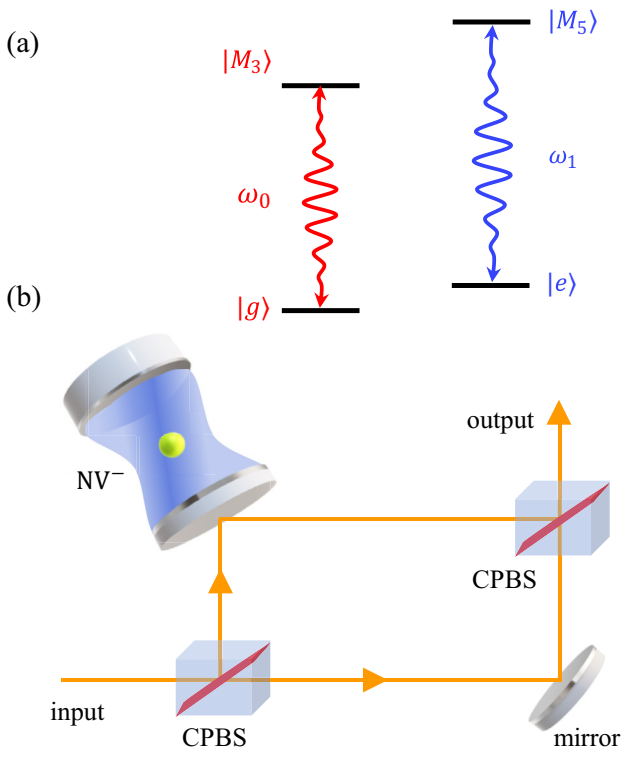

FIG. 1. Quantum memory (QM) for a polarized photon. (a) Relative-level structure and optical transition of an NV$^-$ center; (b) schematic of a quantum controlled-polarization-flip unit that is referred to as a QM with single input and output. Here an NV$^-$ center is coupled to a single-sided cavity; CPBS represents a circularly polarizing beam splitter that reflects photons with polarization $|R\rangle$ and transmits those with $|L\rangle$.

NV$^-$ center in diamond consists of a substitutional nitrogen atom and an adjacent vacancy. Its ground state is an electronic spin triplet with a zero-field splitting of 2.88 GHz between magnetic sublevels for $|m_s = 0\rangle$ and $|m_s = \pm 1\rangle$. When an external magnetic field is applied along the NV$^-$ symmetry axis, it lifts the degeneracy of $|m_s = \pm 1\rangle$ and increases the separation between the states $|g\rangle = |m_s = 0\rangle$ and $|e\rangle = |m_s = +1\rangle$, as well as allowing spin-conserving optical transitions; the NV$^-$ center in states $|g\rangle$ and $|e\rangle$ can be optically excited through a dipole-allowed transition to excited states $|M_3\rangle$ and $|M_5\rangle$ by the absorption of a right circularly polarized photon $|R\rangle$ with resonant frequencies ω_0 and $\omega_1 = \omega_0 + \Delta$, respectively [77]. In practice, a detuning of $\Delta = 2.71$ GHz can be achieved for a magnetic field of $B_z \sim 20$ mT. Note that all other dipole-allowed transitions involving four other excited states (i.e., $|M_1\rangle$, $|M_2\rangle$, $|M_4\rangle$, and $|M_6\rangle$) can be neglected due to optical selection rules or excessive detuning [94–96].

When the cavity mode a, interacting with the NV$^-$ center, is near-resonant with the transition $|g\rangle \leftrightarrow |M_3\rangle$, the reflection of the cavity with the NV$^-$ center in states $|g\rangle$ and $|e\rangle$ will be different for an input photon that is resonant with the cavity: (a) The cavity reflection compared to that of a bare cavity will be significantly modified by destructive interference [97], inhibiting the photon from entering the cavity, if the NV$^-$ center is in state $|g\rangle$; (b) however, the cavity reflection will

remain unaffected if the NV^- center is in state $|e\rangle$ and its dipole-allowed transition is largely detuned from the cavity by Δ. Therefore, an R-polarized photon with frequency ω impinging on an NV^--center–cavity system can be scattered into the output port with a state-dependent reflection coefficient that is determined by the state of the NV^- center.

The scattering of an NV^--center–cavity system is similar to that of a dipole-cavity system, since two dipole-allowed transitions are spin conserving and decoupled from each other. Meanwhile, the reflection coefficient of a dipole-cavity system can be obtained by solving the dynamic equations of the system (cavity mode a and Pauli spin operator σ_- or σ_z) in combination with the standard input-output relation [36–38],

$$\begin{aligned}\frac{da}{dt} &= -[i(\omega_c-\omega)+\frac{\kappa}{2}]a - g\sigma_- - \sqrt{\kappa_c}\,a_{\rm in} + N,\\ \frac{d\sigma_-}{dt} &= -[i(\omega_s-\omega)+\frac{\gamma}{2}]\sigma_- - g\sigma_z\,a + N',\\ a_{\rm out} &= a_{\rm in} + \sqrt{\kappa_c}\,a,\end{aligned} \tag{1}$$

where ω_s (ω_c) is the dipole-transition (cavity-mode) frequency, $\kappa = \kappa_c + \kappa_l$ is the cavity total loss, κ_c describes a directional coupling between the cavity mode and the input and output modes, κ_l describes the loss rate coupling to nonguided modes, g represents the coupling between the dipole and the cavity, and γ is the decay rate of the excited state. The operators N and N' represent noises and are used to preserve the desired commutation relations, whereas $a_{\rm in}$ ($a_{\rm out}$) is the input (output) mode.

In the weak excitation limit, the dipole is predominantly in the ground state at most times and we can take $\langle\sigma_z\rangle \simeq -1$. The reflection coefficient in the frequency domain can be described as [38]

$$r_s(\omega) = 1 - \frac{2\beta(i\Delta_s+1)}{(i\Delta_s+1)(i\Delta_c+1)+C}, \tag{2}$$

where $C = 4g^2/\kappa\gamma$ is the cooperativity, $\beta = \kappa_c/\kappa$ represents the probability factor that the scattering of a dipole-cavity system channels an input photon into the desired output mode, and $\Delta_s = 2(\omega_s-\omega)/\gamma$ and $\Delta_c = 2(\omega_c-\omega)/\kappa$ are effective detunings of the dipole and cavity mode from the input field frequency. For an input R-polarized photon with near-resonant frequency $\omega \simeq \omega_c$ (i.e., $\Delta_c \simeq 0$) and a negligible nonguided loss of the dipole-cavity system (i.e., $\beta = 1$), the reflection coefficient $r_s(\omega)$ can be simplified to $r_s = 1 - 2/(1+\delta C)$ with $\delta = 1/(i\Delta_s+1)$. We have $r_0 \simeq 1$ when $C \gg \max(\Delta_s, 1)$ is satisfied, whereas we have $r_1 \simeq -1$ when $\Delta_s \gg \max(C, 1)$ or $C \simeq 0$ is satisfied.

For an NV^--center–cavity system with $\omega_0 \simeq \omega_c$, an R-polarized photon with frequency $\omega \simeq \omega_c$ impinging on it, in principle, can be scattered into the output port with $r_0 \simeq 1$ ($r_1 \simeq -1$) if the NV^- center is in state $|g\rangle$ ($|e\rangle$); the state-dependent reflection coefficient of an NV^--center–cavity system is determined by the state of the NV^- center. Moreover, new types of color centers in diamond, consisting of two carbon vacancies between which is a group IV atom [83,98], have a four-level structure, shown in Fig. 1, and have been used to enhance quantum communication [84] by coupling to a double-sided optical cavity.

The state-dependent reflection can be used to construct a controlled-polarization-flip (CPF) unit using the NV^- center as the control and the photon polarization as the target [80], shown in Fig. 1(b). The CPF unit consists of a cavity–NV^--center system and two circularly polarizing beam splitters (CPBSs) that reflect (transmit) photons in the right (left) circularly polarized state $|R\rangle$ ($|L\rangle$). Suppose an arbitrary polarized photon p is in state $|\Psi_p\rangle = \alpha_1|D\rangle + \beta_1|A\rangle$, where $|D\rangle = (|L\rangle + |R\rangle)/\sqrt{2}$ and $|A\rangle = (|L\rangle - |R\rangle)/\sqrt{2}$ are linearly polarized and orthogonal; the NV^- center embedded in a cavity is initialized to $|\Psi_s\rangle = \alpha_2|g\rangle + \beta_2|e\rangle$ with $|\alpha_i|^2 + |\beta_i|^2 = 1$ ($i = 1, 2$). The photon p input into the CPF unit arrives at the first CPBS that reflects the $|R\rangle$ component of photon p and transmits the $|L\rangle$ one. The $|R\rangle$ component is then reflected by the NV^--center–cavity system, introducing different phase shifts for the NV^- center in states $|g\rangle$ and $|e\rangle$; however, the $|L\rangle$ component is reflected by a mirror. The combined state of the NV^- center and photon p evolves to

$$\begin{aligned}|\Psi_c'\rangle = \frac{1}{\sqrt{2}}[&(\alpha_1-\beta_1)|R_r\rangle(\alpha_2|g\rangle - \beta_2|e\rangle)\\ &+(\alpha_1+\beta_1)|L_t\rangle(\alpha_2|g\rangle + \beta_2|e\rangle)],\end{aligned} \tag{3}$$

where the subscript r (t) represents that photon p is in the reflection (transmission) mode of the first CPBS. The two photonic components in both spatial modes are recombined at the second CPBS and are simultaneously directed into the output port when their optical paths between two CPBSs are equal. Finally, the combined state of photon p and the NV^- center evolves into the desired output state of the CPF unit as

$$|\Psi_c\rangle = \alpha_2|g\rangle|\Psi_p\rangle + \beta_2|e\rangle|\bar{\Psi}_p\rangle, \tag{4}$$

where $|\bar{\Psi}_p\rangle = \alpha_1|A\rangle + \beta_1|D\rangle$ has the same form as that of $|\Psi_p\rangle$, except the polarization-flip $|D\rangle \leftrightarrow |A\rangle$. This unit, referred to as a QM below, constitutes an elementary building block for distributed entanglement generation that is enhanced by the time-bin qudit encoding with inherent quantum multiplexing.

III. PROTOCOL FOR ENTANGLING THREE PAIRS OF QUANTUM MEMORIES WITH A SINGLE PHOTON

So far, we have described an effective CPF unit (i.e., QM) between the NV^--center electron spin and polarized photons. In this section, we describe a method entangling three QMs (QM1, QM3, and QM5) in one node with three QMs (QM2, QM4, and QM6) in a distant node using a polarized photon with four time bins. As shown in Fig. 2, the setup is composed of half-wave plates (Hs), polarizing beam splitters (PBSs), and optical switchers (OSs) as well as QMs. The OS_i ($i = 1, \ldots, 6$) can direct two spatial modes of photons with different time bins into one spatial mode, and vice versa; PBS_i (PBS_i') transmits photons with polarization $|D\rangle$ ($|A\rangle$) and reflects those with $|A\rangle$ ($|D\rangle$); H flips the polarization of photons passing it and performs the conversion $|A\rangle \leftrightarrow |D\rangle$. In general, this protocol consists of two main procedures: (a) In node A, a hybrid entangled state is created between a high-dimensional single photon and three two-dimensional QMs. Subsequently, the photon is transmitted to the distant node B. (b) Upon receiving this photon, node B converts the

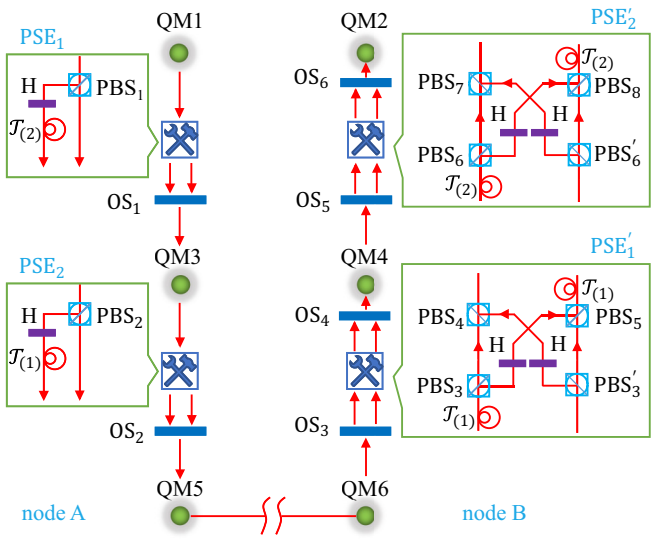

FIG. 2. Schematics of entangling three pairs of quantum memories. Here QMi ($i = 1, \ldots, 6$) denotes a quantum memory implemented by a CPF unit, shown in Fig. 1(b); OS$_i$ ($i = 1, \ldots, 6$) is an optical switch that directs two spatial modes of a photon with different time bins into one spatial mode, and vice versa; PBS$_i$ (PBS$'_i$) represents a polarizing beam splitter that transmits photons with polarization $|D\rangle$ ($|A\rangle$) and reflects those with $|A\rangle$ ($|D\rangle$); a half-wave plate H flips the polarization of photons passing it and performs the conversion $|A\rangle \leftrightarrow |D\rangle$; $\mathcal{T}_{(k)}$ is a time delay operator that introduces an optical delay of kt_Δ; PSE$_i$ and PSE$'_i$ ($i = 1, 2$) represent photon-state engineering blocks.

hybrid entanglement into three two-QM entanglements, which is heralded by the detection of a single photon.

A. Hybrid entanglement of a high-dimensional single photon and three QMs

Suppose QMi ($i = 1, \ldots, 6$) is initialized to the superposition state $|\Psi_i\rangle = (|g_i\rangle + |e_i\rangle)/\sqrt{2}$ and an input photon P with D polarization is impinged on QM1. We can obtain the combined state of the photon and QM1, according to Eq. (4), as

$$|\Phi_1\rangle = \frac{1}{\sqrt{2}}(\mathcal{T}_{(0)}|g_1\rangle|D\rangle + \mathcal{T}_{(0)}|e_1\rangle|A\rangle), \tag{5}$$

where $\mathcal{T}_{(k)}$ represents an operator that introduces a time delay of kt_Δ and satisfies the relation $\mathcal{T}_{(i+j)} = \mathcal{T}_{(i)}\mathcal{T}_{(j)}$; the time delay t_Δ equals the time interval between two neighboring time bins. The photon then passes through a photon-state engineering (PSE) circuit composed of PBS$_1$ and H, which is followed by time delay $\mathcal{T}_{(2)}$. Its polarization difference is converted into that of time bins, performing $\mathcal{T}_{(0)}|A\rangle \to \mathcal{T}_{(2)}|D\rangle$. Subsequently, the two time bins of photon P in two spatial modes are combined into one spatial mode by OS$_1$ and are impinged into QM3.

The combined state of two QMs and photon P evolves into

$$|\Phi_2\rangle = \frac{1}{2}\sum_{i=0}^{2}\mathcal{T}_3^{(i,2)}|g_1g_3\rangle|D\rangle, \tag{6}$$

where $\mathcal{T}_3^{(i,2)}$ ($i = 0, 1, 2$) flips the state of i QMs and is represented by

$$\mathcal{T}_3^{(0,2)} = \mathcal{T}_{(0)}, \quad \mathcal{T}_3^{(1,2)} = \mathcal{T}_{(2)}\sigma_1^X + \mathcal{T}_{(0)}\sigma_P^X\sigma_3^X,$$
$$\mathcal{T}_3^{(2,2)} = \mathcal{T}_{(2)}\sigma_P^X\sigma_1^X\sigma_3^X. \tag{7}$$

Here $\sigma_P^X = |D\rangle\langle A| + |A\rangle\langle D|$ flips the polarization of photon P and $\sigma_i^X = |g_i\rangle\langle e_i| + |e_i\rangle\langle g_i|$ flips the state of QMi. Note that an implicit identity consisting of $\sigma_P^I = |D\rangle\langle D| + |A\rangle\langle A|$ and $\sigma_i^I = |g_i\rangle\langle g_i| + |e_i\rangle\langle e_i|$ is omitted in $\mathcal{T}_3^{(0,2)}$ and $\mathcal{T}_3^{(1,2)}$ and in similar operators hereafter when there is no confusion.

Photon P then enters the PSE$_2$ circuit consisting of PBS$_2$ and H, which is followed by time delay $\mathcal{T}_{(1)}$. The A-polarization modes are converted into D-polarization modes with different time bins, i.e., $\mathcal{T}_{(0)}|A\rangle \to \mathcal{T}_{(1)}|D\rangle$ or $\mathcal{T}_{(2)}|A\rangle \to \mathcal{T}_{(3)}|D\rangle$, which, in combination with $\mathcal{T}_{(0)}|D\rangle$ and $\mathcal{T}_{(2)}|D\rangle$, are directed into the same spatial mode. After the photon is scattered by QM5, the combined state of three QMs and photon P evolves into a hybrid entangled state,

$$|\Phi_3\rangle = \frac{1}{2\sqrt{2}}\sum_{i=0}^{3}\mathcal{T}_3^{(i,3)}|g_1g_3g_5\rangle|D\rangle, \tag{8}$$

where the operators $\mathcal{T}_3^{(i,3)}$ ($i = 0, 1, 2, 3$) can be described as

$$\mathcal{T}_3^{(0,3)} = \mathcal{T}_{(0)}, \quad \mathcal{T}_3^{(1,3)} = \mathcal{T}_{(2)}\sigma_1^X + \mathcal{T}_{(1)}\sigma_3^X + \mathcal{T}_{(0)}\sigma_P^X\sigma_5^X,$$
$$\mathcal{T}_3^{(2,3)} = \mathcal{T}_{(3)}\sigma_1^X\sigma_3^X + \mathcal{T}_{(2)}\sigma_P^X\sigma_1^X\sigma_5^X + \mathcal{T}_{(1)}\sigma_P^X\sigma_3^X\sigma_5^X,$$
$$\mathcal{T}_3^{(3,3)} = \mathcal{T}_{(3)}\sigma_P^X\sigma_1^X\sigma_3^X\sigma_5^X. \tag{9}$$

It is easy to check that the total dimension of the polarization and time bin of photon P is eight and each basis state is exclusively correlated with one of eight product states of three QMs. Photon P is transmitted to the distant node B and interacts with the circuit shown in the right panel in Fig. 2 to entangle three pairs of QMs situated in two nodes. In principle, each QM pair (QMi,QMj) can be in any one of four Bell states as follows:

$$|\phi_{ij}^{\pm}\rangle = \frac{1}{\sqrt{2}}(|g_i\rangle|g_j\rangle \pm |e_i\rangle|e_j\rangle),$$
$$|\psi_{ij}^{\pm}\rangle = \frac{1}{\sqrt{2}}(|e_i\rangle|g_j\rangle \pm |g_i\rangle|e_j\rangle). \tag{10}$$

B. Heralded entanglement of three pairs of QMs

Upon arriving at the distant node B, the photon is directed to interact with QM6. The combined state of four QMs and photon P evolves into

$$|\Phi_4\rangle = \frac{1}{2\sqrt{2}}\sum_{i=0}^{3}\mathcal{T}_{3,1}^{(i,3)}|g_1g_3\phi_{5,6}^{+}\rangle|D\rangle, \tag{11}$$

where QM5 and QM6 can be maximally entangled in state $|\phi_{5,6}^{+}\rangle$ or $|\psi_{5,6}^{+}\rangle$ if photon P is measured in the basis spanned by two polarization states ($|D\rangle$ and $|A\rangle$) in combination with four time bins [i.e., $\mathcal{T}_{(0)}$, $\mathcal{T}_{(1)}$, $\mathcal{T}_{(2)}$, and $\mathcal{T}_{(3)}$], and the operators $\mathcal{T}_{3,1}^{(i,3)}$ ($i = 0, 1, 2, 3$) can be described as

$$\mathcal{T}_{3,1}^{(0,3)} = \mathcal{T}_{(0)}, \quad \mathcal{T}_{3,1}^{(1,3)} = \mathcal{T}_{(2)}\sigma_1^X + \mathcal{T}_{(1)}\sigma_3^X + \mathcal{T}_{(0)}\sigma_P^X\sigma_6^X,$$
$$\mathcal{T}_{3,1}^{(2,3)} = \mathcal{T}_{(3)}\sigma_1^X\sigma_3^X + \mathcal{T}_{(2)}\sigma_P^X\sigma_1^X\sigma_6^X + \mathcal{T}_{(1)}\sigma_P^X\sigma_3^X\sigma_6^X,$$
$$\mathcal{T}_{3,1}^{(3,3)} = \mathcal{T}_{(3)}\sigma_P^X\sigma_1^X\sigma_3^X\sigma_6^X. \tag{12}$$

To entangle QM3 and QM4, photon P is sent to OS_3 and its time bins with $\mathcal{T}_{(0)}$ and $\mathcal{T}_{(2)}$ [$\mathcal{T}_{(1)}$ and $\mathcal{T}_{(3)}$] are directed into the left (right) mode of PSE'_1. The PSE'_1 switches the photon states $\mathcal{T}_{(0)}|A\rangle$ and $\mathcal{T}_{(2)}|A\rangle$ with $\mathcal{T}_{(1)}|D\rangle$ and $\mathcal{T}_{(3)}|D\rangle$, respectively. All time bins of photon P are then combined into one spatial mode by OS_4 and directed to interact with QM4. Therefore, the combined state of five QMs and photon P, just before photon P enters OS_5, evolves into

$$|\Phi_5\rangle = \frac{1}{2\sqrt{2}} \sum_{i=0}^{3} \mathcal{T}_{3,2}^{(i,3)} |g_1 \phi_{3,4}^{+} \phi_{5,6}^{+}\rangle |D\rangle, \tag{13}$$

where the operators $\mathcal{T}_{3,2}^{(i,3)}$ $(i = 0, 1, 2, 3)$ can be described as

$$\begin{aligned}
&\mathcal{T}_{3,2}^{(0,3)} = \mathcal{T}_{(0)}, \quad \mathcal{T}_{3,2}^{(1,3)} = \mathcal{T}_{(2)}\sigma_1^X + \mathcal{T}_{(1)}\sigma_6^X + \mathcal{T}_{(0)}\sigma_P^X\sigma_4^X, \\
&\mathcal{T}_{3,2}^{(2,3)} = \mathcal{T}_{(3)}\sigma_1^X\sigma_6^X + \left(\mathcal{T}_{(2)}\sigma_1^X + \mathcal{T}_{(1)}\sigma_6^X\right)\sigma_P^X\sigma_4^X, \\
&\mathcal{T}_{3,2}^{(3,3)} = \mathcal{T}_{(3)}\sigma_P^X\sigma_1^X\sigma_4^X\sigma_6^X.
\end{aligned} \tag{14}$$

Obviously, two pairs of QMs, i.e., (QM3, QM4) and (QM5, QM6), can be maximally entangled from state $|\Phi_5\rangle$ after photon P is properly measured.

Furthermore, QM1 and QM2 can be entangled by photon P with a similar procedure: The time bins $\mathcal{T}_{(0)}$ and $\mathcal{T}_{(1)}$ [$\mathcal{T}_{(2)}$ and $\mathcal{T}_{(3)}$] of photon P are directed into the left (right) mode of PSE'_2, which switches the photon states $\mathcal{T}_{(0)}|A\rangle$ and $\mathcal{T}_{(1)}|A\rangle$ with $\mathcal{T}_{(2)}|D\rangle$ and $\mathcal{T}_{(3)}|D\rangle$, respectively; the four time bins with both D polarization and A polarization are combined into one spatial mode by OS_6 and then are scattered by QM2. Immediately, the combined state of six QMs and photon P after scattering evolves into

$$|\Phi_6\rangle = \frac{1}{2\sqrt{2}} \sum_{i=0}^{3} \mathcal{T}_{3,3}^{(i,3)} |\phi_{1,2}^{+} \phi_{3,4}^{+} \phi_{5,6}^{+}\rangle |D\rangle, \tag{15}$$

where the operators $\mathcal{T}_{3,3}^{(i,3)}$ $(i = 0, 1, 2, 3)$ can be described as

$$\begin{aligned}
&\mathcal{T}_{3,3}^{(0,3)} = \mathcal{T}_{(0)}, \quad \mathcal{T}_{3,3}^{(1,3)} = \mathcal{T}_{(2)}\sigma_4^X + \mathcal{T}_{(1)}\sigma_6^X + \mathcal{T}_{(0)}\sigma_P^X\sigma_2^X, \\
&\mathcal{T}_{3,3}^{(2,3)} = \mathcal{T}_{(3)}\sigma_4^X\sigma_6^X + \left(\mathcal{T}_{(2)}\sigma_4^X + \mathcal{T}_{(1)}\sigma_6^X\right)\sigma_P^X\sigma_2^X, \\
&\mathcal{T}_{3,3}^{(3,3)} = \mathcal{T}_{(3)}\sigma_P^X\sigma_2^X\sigma_4^X\sigma_6^X.
\end{aligned} \tag{16}$$

The state $|\Phi_6\rangle$ can be referred to as a hybrid entangled state with the same form as that of Eq. (8) when each QM pair is confined in a subspace with two basis states, $|\phi_{i,i+1}^{+}\rangle$ and $|\psi_{i,i+1}^{+}\rangle$ $(i = 1, 3, 5)$. The three pairs of QMs can be projected into a product state of three entangled states ($|\phi_{i,i+1}^{+}\rangle$ or $|\psi_{i,i+1}^{+}\rangle$) when photon P is measured in a basis consisting of two polarization states ($|D\rangle$ and $|A\rangle$) in combination with four time bins [i.e., $\mathcal{T}_{(0)}$, $\mathcal{T}_{(1)}$, $\mathcal{T}_{(2)}$, and $\mathcal{T}_{(3)}$]. For instance, the three pairs of QMs will be projected into the state $|\phi_{1,2}^{+}\phi_{3,4}^{+}\phi_{5,6}^{+}\rangle$ ($|\phi_{1,2}^{+}\psi_{3,4}^{+}\psi_{5,6}^{+}\rangle$) when photon P with D polarization is detected in the $\mathcal{T}_{(0)}$ [$\mathcal{T}_{(3)}$] time-bin mode.

IV. PROTOCOL FOR ENTANGLING ($n > 3$) PAIRS OF QUANTUM MEMORIES WITH A SINGLE PHOTON

The time-bin multiplexing method for quantum entanglement creation, in principle, can be generalized to entangle ($n > 3$) pairs of QMs using a single photon. This generalized protocol also consists of two main procedures. In one node, a 2^n-dimensional photon P with two polarization states and $2^{(n-1)}$ time bins entangles with n two-dimensional QMs in a form similar to that described by Eq. (8). In the distant node, the hybrid entangled state is converted into n two-QM entanglements by subsequently entangling each pair of QMs and properly engineering the state of photon P.

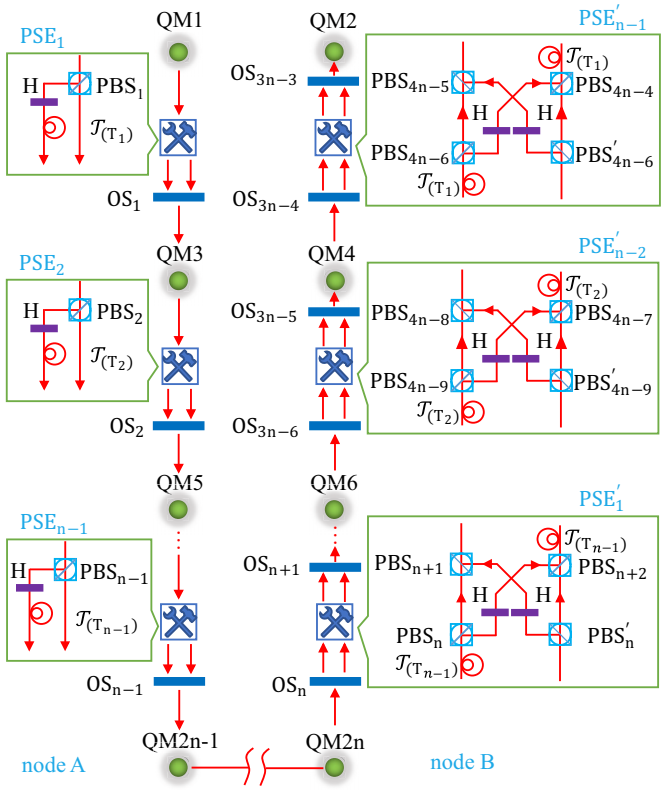

FIG. 3. Schematics of entangling n pairs of quantum memories. Here QMi denotes a quantum memory; OS_i is an optical switch that directs two spatial modes of a photon with different time bins into one spatial mode, and vice versa; PBS_i (PBS'_i) represents a polarizing beam splitter that transmits photons with polarization $|D\rangle$ ($|A\rangle$) and reflects those with $|A\rangle$ ($|D\rangle$); the half-wave plate H flips the polarization of photons passing it and performs the conversion $|A\rangle \leftrightarrow |D\rangle$; $\mathcal{T}_{(T_i)}$ represents a time delay operator that introduces an optical delay of $T_i t_\Delta$ with $T_i = 2^{(n-1-i)}$; PSE_i and PSE'_i represent photon-state engineering blocks.

A. Hybrid entanglement of a high-dimensional single photon and n QMs

Schematics of entangling n pairs of QMs with one photon are shown in Fig. 3. Suppose QMi $(i = 1, 2, \ldots, 2n)$ is initialized in the superposition state $|\Psi_i\rangle = (|g_i\rangle + |e_i\rangle)/\sqrt{2}$. A photon P with D polarization is impinged on QM1 and then is rearranged by PSE_1, which converts $\mathcal{T}_{(0)}|A\rangle$ into $\mathcal{T}_{(T_1)}|D\rangle$. The operator $\mathcal{T}_{(0)}$ is the identity, introducing no delay. Subsequently, OS_1 directs both time bins of photon P into one spatial mode that is then scattered by QM3.

The aforementioned procedure is similar to that involved in the scattering by the mth QM and rearrangement of PSE_m in node A, except that OS_m directs $2^{(m-1)}$ time-bin

components of the D-polarized photon P into one spatial mode. The combined state of photon P and m QMs before the photon is impinged into the $(m+1)$th QM evolves into

$$|\Phi_m\rangle = \frac{1}{\sqrt{2^m}} \sum_{i=0}^{m} \mathcal{T}_n^{(i,m)} |g_1 g_3 \dots g_{2m-1}\rangle |D\rangle, \tag{17}$$

where the operators $\mathcal{T}_n^{(i,m)}$ $(i = 0, 1, \dots, m)$ can be described as

$$\mathcal{T}_n^{(i,m)} = \begin{cases} \mathcal{T}_{(0)}, & i = 0; \\ t_n^i + \sigma_{\mathrm{P}}^X \sigma_{2m-1}^X t_n^{i-1}, & i = 1, 2, \dots, m. \end{cases} \tag{18}$$

Here the ancillary concatenated operator t_n^k $(k = 1, 2, \dots, m)$ flips the state of QM$(2i_j - 1)$ $(j = 1, 2, \dots, k)$ and introduces a time delay $\mathcal{T}_{(T_{i_j})}$ by

$$t_n^k = \sum_{\substack{i_1=1, \\ i_1<i_2<\dots<i_k}}^{m-1} \mathcal{T}_{(T_{i_1})} \mathcal{T}_{(T_{i_2})} \dots \mathcal{T}_{(T_{i_k})} \sigma_{2i_1-1}^X \sigma_{2i_2-1}^X \dots \sigma_{2i_k-1}^X.$$

The PSE$_m$ below the mth QM converts $\mathcal{T}_{(d_l)}|A\rangle \to \mathcal{T}_{(d_l+T_m)}|D\rangle$ for $d_l = 2^{n-m} l$ and $l = 0, 1, \dots, 2^{m-1} - 1$.

After photon P is scattered by the nth QM in node A, the combined state of n QMs and photon P evolves into

$$|\Phi_n\rangle = \frac{1}{\sqrt{2^n}} \sum_{i=0}^{n} \mathcal{T}_n^{(i,n)} |g_1 g_3 \dots g_{2n-1}\rangle |D\rangle, \tag{19}$$

where the operators $\mathcal{T}_n^{(i,n)}$ $(i = 0, 1, \dots, n)$ are of the form defined by Eq. (18). Clearly, $|\Phi_n\rangle$ is a hybrid entangled state, in which a 2^n-dimensional photon entangles with n QMs; the state of n QMs can be projected into a deterministic product state when the photon is properly measured. However, if photon P is transmitted to a distant node B, it will interact with QMs situated there and then entangle n pairs of QMs in a heralded way.

B. Heralded entanglement of n pairs of QMs

Photon P will be immediately scattered by QM2n after it arrives at node B. The combined state of $(n+1)$ QMs and photon P evolves into

$$|\Phi_{n+1}\rangle = \frac{1}{\sqrt{2^n}} \sum_{i=0}^{n} \mathcal{T}_{n,1}^{(i,n)} |g_1 g_3 \dots \phi_{2n-1,2n}\rangle |D\rangle, \tag{20}$$

where $\mathcal{T}_{n,1}^{(i,n)}$ can be described as

$$\mathcal{T}_{n,1}^{(i,n)} = \begin{cases} \mathcal{T}_{(0)}, & i = 0; \\ t_{n,1}^i + \sigma_{\mathrm{P}}^X \sigma_{2n}^X t_{n,1}^{i-1}, & i = 1, 2, \dots, n. \end{cases} \tag{21}$$

Here the operator $t_{n,1}^k$ can be described as

$$t_{n,1}^k = \sum_{\substack{i_1=1, \\ i_1<i_2<\dots<i_k}}^{n-1} \mathcal{T}_{(T_{i_1})} \mathcal{T}_{(T_{i_2})} \dots \mathcal{T}_{(T_{i_k})} \sigma_{2i_1-1}^X \sigma_{2i_2-1}^X \dots \sigma_{2i_k-1}^X.$$

The OS$_n$ directs the time-bin components with $\mathcal{T}_{(0)}, \mathcal{T}_{(2)}, \mathcal{T}_{(4)}, \dots, \mathcal{T}_{(2^{n-1}-2)}$ to the left mode of PSE$_1'$ and those with $\mathcal{T}_{(1)}, \mathcal{T}_{(3)}, \mathcal{T}_{(5)}, \dots, \mathcal{T}_{(2^{n-1}-1)}$ to the right mode of PSE$_1'$. Subsequently, PSE$_1'$ switches the components of $\mathcal{T}_{(2i)}|A\rangle$ with that of $\mathcal{T}_{(2i+1)}|D\rangle$ for $i = 0, 1, \dots, 2^{n-2} - 1$ and then all time-bin components are combined by OS$_n$ and are directed into one spatial mode that interacts with the next QM.

This procedure is similar to that involving the mth QM and PSE$_m'$. For instance, after photon P has been scattered by the mth QM $(1 < m \leqslant n)$, the combined state of photon P and $(n+m)$ QMs can be described as

$$|\Phi_{n+m}\rangle = \frac{1}{\sqrt{2^n}} \sum_{i=0}^{n} \mathcal{T}_{n,m}^{(i,n)} |g_1 g_3 \dots g_{2n-2m-1}\rangle \otimes |\phi_{2n-2m+1,2n-2m+2} \dots \phi_{2n-1,2n}\rangle |D\rangle, \tag{22}$$

where $\mathcal{T}_{n,m}^{(i,n)}$ can be described as

$$\mathcal{T}_{n,m}^{(i,n)} = \begin{cases} \mathcal{T}_{(0)}, & i = 0; \\ t_{n,m}^{(i,n)} + \sigma_{\mathrm{P}}^X \sigma_{2h'}^X t_{n,m}^{(i-1,n)}, & i = 1, 2, \dots, n. \end{cases} \tag{23}$$

Here the operator $t_{n,m}^{(k,n)}$ can be described as

$$t_{n,m}^{(k,n)} = \sum_{i_1=1}^{h} \sum_{i_1<i_2<\dots<i_k}^{h} \mathcal{T}_{(T_{i_1})} \mathcal{T}_{(T_{i_2})} \dots \mathcal{T}_{(T_{i_k})} \otimes \sigma_{2i_1-1}^X \sigma_{2i_2-1}^X \dots \sigma_{2i_k-1}^X + \sum_{i_1=1}^{h} \sum_{i_k=h'}^{n-1} \sum_{i_1<i_2<\dots<i_{k-1}}^{h} \mathcal{T}_{(T_{i_1})} \mathcal{T}_{(T_{i_2})} \dots \mathcal{T}_{(T_{i_k})}$$
$$\otimes \sigma_{2i_1-1}^X \sigma_{2i_2-1}^X \dots \sigma_{2i_{k-1}-1}^X \sigma_{2i_k+2}^X + \sum_{i_1=1}^{h} \sum_{i_{k-1}=h'}^{n-1} \sum_{i_1<i_2<\dots<i_{k-2}}^{h} \sum_{i_{k-1}<i_k}^{n-1} \mathcal{T}_{(T_{i_1})} \mathcal{T}_{(T_{i_2})} \dots$$
$$\otimes \mathcal{T}_{(T_{i_k})} \sigma_{2i_1-1}^X \sigma_{2i_2-1}^X \dots \sigma_{2i_{k-2}-1}^X \sigma_{2i_{k-1}+2}^X \sigma_{2i_k+2}^X + \dots + \sum_{i_1=h'}^{n-1} \sum_{i_1<i_2<\dots<i_k}^{n-1} \mathcal{T}_{(T_{i_1})} \mathcal{T}_{(T_{i_2})} \dots \mathcal{T}_{(T_{i_k})} \otimes \sigma_{2i_1+2}^X \sigma_{2i_2+2}^X \dots \sigma_{2i_k+2}^X,$$

and the parameters h and h' are defined as $h = n - m$ and $h' = n - m + 1$. Obviously, the combined state of $2n$ QMs and photon P, after P has been scattered by QM2, evolves into

$$|\Phi_{2n}\rangle = \frac{1}{\sqrt{2^n}} \sum_{i=0}^{n} \mathcal{T}_{n,n}^{(i,n)} |\phi_{1,2} \phi_{3,4} \dots \phi_{2n-1,2n}\rangle |D\rangle, \tag{24}$$

where $\mathcal{T}_{n,n}^{(i,n)}$ has the same form as $\mathcal{T}_{n,m}^{(i,n)}$, shown in Eq. (23). Therefore, the n pairs of QMs can be projected into a product state consisting of n maximally entangled states, after photon P is properly measured. This heralds the success of entanglement creation between n pairs of QMs using one photon.

V. PERFORMANCE OF THE MULTIPLEXING QUANTUM ENTANGLEMENT CREATION

Our protocol focuses on entangling n pairs of QMs using one high-dimensional encoded single photon. The photon is subsequently scattered by $2n$ QMs, whereas its states are rearranged by linear-optical elements between each two scatterings to introduce more time bins (i.e., PSE_i) or interchange some D-polarization and A-polarization components with a preset delay (i.e., PSE_i'). So far, we have assumed that the interface between the single photon and the QMs is deterministic with unity refection $|r_i| = 1$ and state-dependent phase shift 0 or π. However, the finite cooperativity C and detunings always introduce a deviation from ideal single-photon scattering and affect the fidelity and efficiency of entanglement creation. Meanwhile, the finite losses scattered into nonguided channels lead to a probability factor with $\beta < 1$ and degrade the scattering procedure. For a diamond nanophotonic crystal cavity, these losses can be efficiently suppressed, leading to an effective directional coupling with $\beta \simeq 0.98$ [99,100]. In practice, the influence of the finite probability factor β and cooperativity C as well as finite detunings of the fidelity can be suppressed by properly tuning them. For instance, the state-dependent reflection coefficients $r_0 \simeq -r_1 \simeq 0.96$ with a phase difference of π can be achieved at $\beta = 0.98$, $C = 45$, $\Delta_c = 0.3$, and $\Delta_E = 150$, which lead to a unity fidelity but a decreased efficiency with $\eta_0 = |r_0|^2$ for each single-photon scattering. Note that the transmission of the other path should be modified accordingly in Fig. 1(b). Therefore, the efficiency of entangling n pairs of QMs will be decreased to η_0^{2n}, due to $2n$ single-photon scattering procedures.

The dominant source of photon loss is introduced by the transmission channel linking two nodes. In practice, the channel loss increases exponentially with the distance l between two nodes. The efficiency of our protocol can thus be described as

$$\eta_n = \eta_0^{2n}\eta_d \exp(-\alpha l), \tag{25}$$

where n is the number of QM pairs, η_d is the single-photon detector efficiency and can be as large as $\eta_d \geqslant 0.96$, and α is the attenuation coefficient. Similarly, the efficiency of previous protocols [36–41] for entangling n pairs of QMs, which consume one photon to entangle one pair of QMs, can be described as

$$\eta_n^s = \eta_0^{2n}\eta_d^n \exp(-n\alpha l). \tag{26}$$

The efficiencies of our protocol for generating $n = 3$ and $n = 10$ pairs of QMs are shown in Fig. 4 as a function of the distance l between two nodes. The corresponding efficiencies of previous protocols with the same parameters are also shown in Fig. 4. The channel is assumed to be an optical fiber of attenuation 0.2 dB/km ($\alpha \simeq 1/22$ km^{-1}). The efficiency of the single-photon detector is assumed to be $\eta_d = 0.96$. For QMs situated in the same node with a negligible distance $l \simeq 0$, we can entangle $n = 3$ ($n = 10$) pairs of QMs with efficiencies $\eta_3 = 0.588$ and $\eta_{10} = 0.183$, which are larger than the corresponding efficiencies $\eta_3' = 0.543$ and $\eta_{10}' = 0.130$ achieved by entangling n pairs of QMs with n photons, due to the finite efficiency of single-photon detectors and single-photon scattering. For a medium distance $l = 22$ km, we can entangle $n = 3$ ($n = 10$) pairs of QMs with efficiencies $\eta_3 = 0.217$ and $\eta_{10} = 0.069$, which exceed the efficiencies $\eta_3' = 0.027$ and $\eta_{10}' = 5.92 \times 10^{-6}$ by one and four orders of magnitude, respectively. Furthermore, this efficiency enhancement can be increased further for larger n and l.

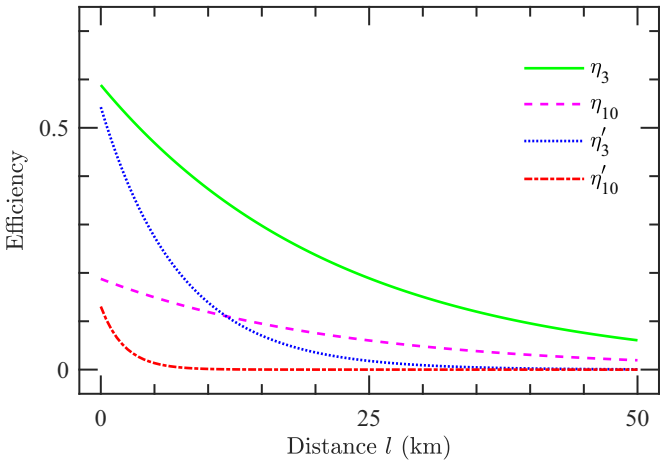

FIG. 4. Efficiency of entanglement creation for n pairs of QMs versus distance l. Here η_3 and η_{10} represent the efficiencies of our protocol using time-bin multiplexing for $n = 3$ and $n = 10$, whereas η_3' and η_{10}' represent the corresponding efficiencies of previous protocols described by Eq. (26). The efficiency of the single-photon detector is assumed to be $\eta_d = 0.96$; the channel attenuation coefficient is $\alpha \simeq 1/22$ (i.e., 0.2 dB/km).

VI. DISCUSSION AND SUMMARY

This protocol generalizes previous entanglement creation with quantum multiplexing using a time-bin qubit [42] to a high-dimensional time-bin qudit. Two distant nodes, in principle, can entangle multiple ($n \geqslant 3$) pairs of QMs using a single photon encoded in two polarization modes and $2^{(n-1)}$ time bins. Therefore, it is necessary to deterministically distinguish these time bins and properly measure them with single-photon detectors [79]. In practice, these processes can be completed by fast optical switching that directs each time bin into a desired spatial mode. Such switching devices can be fabricated with schemes based on subnanosecond phase control in Mach-Zehnder interferometers, which have been demonstrated using electro-optic modulation for a variety of material platforms [101,102]. Although our proposal is detailed with the NV$^-$-center–cavity system, it could also be implemented with other spin-photon interfaces [63–65].

In summary, we have proposed a multiplexing protocol for generating quantum entanglement between distant QMs. We can simultaneously entangle multiple pairs of QMs by using a single photon with a time-bin qudit due to its inherent quantum multiplexing. The main idea of our entanglement creation proposal is similar to the original one, which generates hybrid quantum entanglement between a photon qubit and a stationary qubit (i.e., QM) and causes the photon to interact with another QM to entangle two QMs, but our proposal first entangles a photon qudit and multiple QMs and then converts the hybrid entanglement into parallel entanglements

between QM pairs by subsequently interacting the photon qudit with some other QMs. This leads to a significant efficiency enhancement of distant entanglement creation and can find its application in long-distance quantum communication and quantum networks.

ACKNOWLEDGMENTS

This work was supported by the National Natural and Science Foundation of China (Grant No. 11904171) and the Natural Science Foundation of Jiangsu Province (Grant No. BK20180461).

[1] S. Wehner, D. Elkouss, and R. Hanson, Quantum internet: A vision for the road ahead, Science **362**, eaam9288 (2018).

[2] I. M. Georgescu, S. Ashhab, and F. Nori, Quantum simulation, Rev. Mod. Phys. **86**, 153 (2014).

[3] T. Li, Z. Gao, and Z. Li, Measurement-device-independent quantum secure direct communication: Direct quantum communication with imperfect measurement device and untrusted operator, Europhys. Lett. **131**, 60001 (2020).

[4] T. Li and G.-L. Long, Quantum secure direct communication based on single-photon Bell-state measurement, New J. Phys. **22**, 063017 (2020).

[5] F.-G. Deng, G. L. Long, and X.-S. Liu, Two-step quantum direct communication protocol using the Einstein-Podolsky-Rosen pair block, Phys. Rev. A **68**, 042317 (2003).

[6] F. Xu, X. Ma, Q. Zhang, H.-K. Lo, and J.-W. Pan, Secure quantum key distribution with realistic devices, Rev. Mod. Phys. **92**, 025002 (2020).

[7] Z. Gao, T. Li, and Z. Li, Long-distance measurement-device–independent quantum secure direct communication, EPL **125**, 40004 (2019).

[8] F. Massa, A. Moqanaki, F. Del Santo, B. Dakic, and P. Walther, Experimental two-way communication with one photon, Adv. Quantum Technol. **2**, 1900050 (2019).

[9] Z.-R. Zhou, Y.-B. Sheng, P.-H. Niu, L.-G. Yin, G.-L. Long, and L. Hanzo, Measurement-device-independent quantum secure direct communication, Sci. China Phys. Mech. Astron. **63**, 230362 (2020).

[10] L. Zhou, Y.-B. Sheng, and G.-L. Long, Device-independent quantum secure direct communication against collective attacks, Sci. Bull. **65**, 12 (2020).

[11] J. I. Cirac, A. K. Ekert, S. F. Huelga, and C. Macchiavello, Distributed quantum computation over noisy channels, Phys. Rev. A **59**, 4249 (1999).

[12] Y. L. Lim, A. Beige, and L. C. Kwek, Repeat-Until-Success Linear Optics Distributed Quantum Computing, Phys. Rev. Lett. **95**, 030505 (2005).

[13] W. Qin, X. Wang, A. Miranowicz, Z. Zhong, and F. Nori, Heralded quantum controlled-phase gates with dissipative dynamics in macroscopically distant resonators, Phys. Rev. A **96**, 012315 (2017).

[14] I. Cohen and K. Mølmer, Deterministic quantum network for distributed entanglement and quantum computation, Phys. Rev. A **98**, 030302(R) (2018).

[15] S. Perseguers, G. Lapeyre, Jr., D. Cavalcanti, M. Lewenstein, and A. Acín, Distribution of entanglement in large-scale quantum networks, Rep. Prog. Phys. **76**, 096001 (2013).

[16] W. Qin and F. Nori, Controllable single-photon transport between remote coupled-cavity arrays, Phys. Rev. A **93**, 032337 (2016).

[17] N. Gisin, G. Ribordy, W. Tittel, and H. Zbinden, Quantum cryptography, Rev. Mod. Phys. **74**, 145 (2002).

[18] H.-J. Briegel, W. Dür, J. I. Cirac, and P. Zoller, Quantum Repeaters: The Role of Imperfect Local Operations in Quantum Communication, Phys. Rev. Lett. **81**, 5932 (1998).

[19] T.-J. Wang, S.-Y. Song, and G. L. Long, Quantum repeater based on spatial entanglement of photons and quantum-dot spins in optical microcavities, Phys. Rev. A **85**, 062311 (2012).

[20] W. J. Munro, A. M. Stephens, S. J. Devitt, K. A. Harrison, and K. Nemoto, Quantum communication without the necessity of quantum memories, Nat. Photon. **6**, 777 (2012).

[21] Y.-B. Sheng, L. Zhou, and G.-L. Long, Hybrid entanglement purification for quantum repeaters, Phys. Rev. A **88**, 022302 (2013).

[22] M. Żukowski, A. Zeilinger, M. A. Horne, and A. K. Ekert, "Event-Ready-Detectors" Bell Experiment Via Entanglement Swapping, Phys. Rev. Lett. **71**, 4287 (1993).

[23] L. Chen and W. She, Hybrid entanglement swapping of photons: Creating the orbital angular momentum Bell states and Greenberger-Horne-Zeilinger states, Phys. Rev. A **83**, 012306 (2011).

[24] Y.-N. Chen, S.-L. Chen, N. Lambert, C.-M. Li, G.-Y. Chen, and F. Nori, Entanglement swapping and testing quantum steering into the past via collective decay, Phys. Rev. A **88**, 052320 (2013).

[25] X. Su, C. Tian, X. Deng, Q. Li, C. Xie, and K. Peng, Quantum Entanglement Swapping Between Two Multipartite Entangled States, Phys. Rev. Lett. **117**, 240503 (2016).

[26] C. H. Bennett, G. Brassard, S. Popescu, B. Schumacher, J. A. Smolin, and W. K. Wootters, Purification of Noisy Entanglement and Faithful Teleportation Via Noisy Channels, Phys. Rev. Lett. **76**, 722 (1996).

[27] Y.-B. Sheng, F.-G. Deng, and H.-Y. Zhou, Efficient polarization-entanglement purification based on parametric down-conversion sources with cross-Kerr nonlinearity, Phys. Rev. A **77**, 042308 (2008).

[28] Y.-B. Sheng and F.-G. Deng, Deterministic entanglement purification and complete nonlocal Bell-state analysis with hyperentanglement, Phys. Rev. A **81**, 032307 (2010).

[29] X.-M. Hu, C.-X. Huang, Y.-B. Sheng, L. Zhou, B.-H. Liu, Y. Guo, C. Zhang, W.-B. Xing, Y.-F. Huang, C.-F. Li, and G.-C. Guo, Long-Distance Entanglement Purification for Quantum Communication, Phys. Rev. Lett. **126**, 010503 (2021).

[30] L. Jiang, J. M. Taylor, A. S. Sørensen, and M. D. Lukin, Distributed quantum computation based on small quantum registers, Phys. Rev. A **76**, 062323 (2007).

[31] T. Northup and R. Blatt, Quantum information transfer using photons, Nat. Photon. **8**, 356 (2014).

[32] L. M. Duan, M. D. Lukin, J. I. Cirac, and P. Zoller, Long-distance quantum communication with atomic ensembles and linear optics, Nature (London) **414**, 413 (2001).

[33] E. Togan, Y. Chu, A. S. Trifonov, L. Jiang, J. Maze, L. Childress, M. V. G. Dutt, A. S. Sørensen, P. R. Hemmer,

A. S. Zibrov, and M. D. Lukin, Quantum entanglement between an optical photon and a solid-state spin qubit, Nature (London) **466**, 730 (2010).

[34] B. Hensen, H. Bernien, A. E. Dréau, A. Reiserer, N. Kalb, M. S. Blok, J. Ruitenberg, R. F. Vermeulen, R. N. Schouten, C. Abellán, W. Amaya, V. Pruneri, M. W. Mitchell, M. Markham, D. J. Twitchen, D. Elkouss, S. Wehner, T. H. Taminiau, and R. Hanson, Loophole-free Bell inequality violation using electron spins separated by 1.3 kilometres, Nature (London) **526**, 682 (2015).

[35] J. Borregaard, A. S. Sørensen, and P. Lodahl, Quantum networks with deterministic spin-photon interfaces, Adv. Quantum Technol. **2**, 1800091 (2019).

[36] C. Y. Hu, A. Young, J. L. O'Brien, W. J. Munro, and J. G. Rarity, Giant optical Faraday rotation induced by a single-electron spin in a quantum dot: Applications to entangling remote spins via a single photon, Phys. Rev. B **78**, 085307 (2008).

[37] J.-H. An, M. Feng, and C. H. Oh, Quantum-information processing with a single photon by an input-output process with respect to low-Q cavities, Phys. Rev. A **79**, 032303 (2009).

[38] A. Reiserer and G. Rempe, Cavity-based quantum networks with single atoms and optical photons, Rev. Mod. Phys. **87**, 1379 (2015).

[39] C. Wang, Y. Zhang, and G.-S. Jin, Entanglement purification and concentration of electron-spin entangled states using quantum-dot spins in optical microcavities, Phys. Rev. A **84**, 032307 (2011).

[40] Y.-H. Kang, Y. Xia, and P.-M. Lu, Effective scheme for preparation of a spin-qubit Greenberger–Horne–Zeilinger state and W state in a quantum-dot-microcavity system, J. Opt. Soc. Am. B **32**, 1323 (2015).

[41] T. Li, A. Miranowicz, X. Hu, K. Xia, and F. Nori, Quantum memory and gates using a Λ-type quantum emitter coupled to a chiral waveguide, Phys. Rev. A **97**, 062318 (2018).

[42] N. Lo Piparo, W. J. Munro, and K. Nemoto, Quantum multiplexing, Phys. Rev. A **99**, 022337 (2019).

[43] C. Cabrillo, J. I. Cirac, P. García-Fernández, and P. Zoller, Creation of entangled states of distant atoms by interference, Phys. Rev. A **59**, 1025 (1999).

[44] C.-S. Yu, X. X. Yi, H.-S. Song, and D. Mei, Robust preparation of Greenberger-Horne-Zeilinger and W states of three distant atoms, Phys. Rev. A **75**, 044301 (2007).

[45] T. Li and F.-G. Deng, Error-rejecting quantum computing with solid-state spins assisted by low-Q optical microcavities, Phys. Rev. A **94**, 062310 (2016).

[46] S. Mahmoodian, P. Lodahl, and A. S. Sørensen, Quantum Networks with Chiral-Light-Matter Interaction in Waveguides, Phys. Rev. Lett. **117**, 240501 (2016).

[47] Z. Yan, Y. Liu, J. Yan, and X. Jia, Deterministically entangling multiple remote quantum memories inside an optical cavity, Phys. Rev. A **97**, 013856 (2018).

[48] D. L. Hurst, K. B. Joanesarson, J. Iles-Smith, J. Mørk, and P. Kok, Generating Maximal Entanglement Between Spectrally Distinct Solid-State Emitters, Phys. Rev. Lett. **123**, 023603 (2019).

[49] F.-G. Deng, B.-C. Ren, and X.-H. Li, Quantum hyperentanglement and its applications in quantum information processing, Sci. Bull. **62**, 46 (2017).

[50] M. Erhard, M. Krenn, and A. Zeilinger, Advances in high-dimensional quantum entanglement, Nat. Rev. Phys. **2**, 365 (2020).

[51] G. A. Howland and J. C. Howell, Efficient High-Dimensional Entanglement Imaging with a Compressive-Sensing Double-Pixel Camera, Phys. Rev. X **3**, 011013 (2013).

[52] X.-M. Hu, J.-S. Chen, B.-H. Liu, Y. Guo, Y.-F. Huang, Z.-Q. Zhou, Y.-J. Han, C.-F. Li, and G.-C. Guo, Experimental Test of Compatibility-Loophole-Free Contextuality with Spatially Separated Entangled Qutrits, Phys. Rev. Lett. **117**, 170403 (2016).

[53] J. Daboul, X. Wang, and B. C. Sanders, Quantum gates on hybrid qudits, J. Phys. A **36**, 2525 (2003).

[54] A. M. Yao and M. J. Padgett, Orbital angular momentum: Origins, behavior and applications, Adv. Opt. Photon. **3**, 161 (2011).

[55] B. Brecht, D. V. Reddy, C. Silberhorn, and M. G. Raymer, Photon Temporal Modes: A Complete Framework for Quantum Information Science, Phys. Rev. X **5**, 041017 (2015).

[56] F. Brandt, M. Hiekkamäki, F. Bouchard, M. Huber, and R. Fickler, High-dimensional quantum gates using full-field spatial modes of photons, Optica **7**, 98 (2020).

[57] X. Gao, M. Erhard, A. Zeilinger, and M. Krenn, Computer-Inspired Concept for High-Dimensional Multipartite Quantum Gates, Phys. Rev. Lett. **125**, 050501 (2020).

[58] W.-Q. Liu, H.-R. Wei, and L.-C. Kwek, Low-Cost Fredkin Gate with Auxiliary Space, Phys. Rev. Appl. **14**, 054057 (2020).

[59] I. Ali-Khan, C. J. Broadbent, and J. C. Howell, Large-Alphabet Quantum Key Distribution Using Energy-Time Entangled Bipartite States, Phys. Rev. Lett. **98**, 060503 (2007).

[60] M. Kues, C. Reimer, P. Roztocki, L. R. Cortés, S. Sciara, B. Wetzel, Y. Zhang, A. Cino, S. T. Chu, B. E. Little, D. J. Moss, L. Caspani, J. Azaña, and R. Morandotti, On-chip generation of high-dimensional entangled quantum states and their coherent control, Nature (London) **546**, 622 (2017).

[61] Z. Zhang, J. Mower, D. Englund, F. N. C. Wong, and J. H. Shapiro, Unconditional Security of Time-Energy Entanglement Quantum Key Distribution using Dual-Basis Interferometry, Phys. Rev. Lett. **112**, 120506 (2014).

[62] S. Ecker, F. Bouchard, L. Bulla, F. Brandt, O. Kohout, F. Steinlechner, R. Fickler, M. Malik, Y. Guryanova, R. Ursin, and M. Huber, Overcoming Noise in Entanglement Distribution, Phys. Rev. X **9**, 041042 (2019).

[63] I. Buluta, S. Ashhab, and F. Nori, Natural and artificial atoms for quantum computation, Rep. Prog. Phys. **74**, 104401 (2011).

[64] D. D. Awschalom, R. Hanson, J. Wrachtrup, and B. B. Zhou, Quantum technologies with optically interfaced solid-state spins, Nat. Photon. **12**, 516 (2018).

[65] E. Janitz, M. K. Bhaskar, and L. Childress, Cavity quantum electrodynamics with color centers in diamond, Optica **7**, 1232 (2020).

[66] P.-B. Li, Z.-L. Xiang, P. Rabl, and F. Nori, Hybrid Quantum Device with Nitrogen-Vacancy Centers in Diamond Coupled to Carbon Nanotubes, Phys. Rev. Lett. **117**, 015502 (2016).

[67] L. Childress, J. M. Taylor, A. S. Sørensen, and M. D. Lukin, Fault-Tolerant Quantum Communication Based on Solid-State Photon Emitters, Phys. Rev. Lett. **96**, 070504 (2006).

[68] S. J. Devitt, A. D. Greentree, R. Ionicioiu, J. L. O'Brien, W. J. Munro, and L. C. L. Hollenberg, Photonic module: An on-demand resource for photonic entanglement, Phys. Rev. A **76**, 052312 (2007).

[69] A. Zheng, J. Li, R. Yu, X.-Y. Lü, and Y. Wu, Generation of Greenberger-Horne-Zeilinger state of distant diamond nitrogen-vacancy centers via nanocavity input-output process, Opt. Express **20**, 16902 (2012).

[70] L.-Y. Cheng, H.-F. Wang, S. Zhang, and K.-H. Yeon, Quantum state engineering with nitrogen-vacancy centers coupled to low-Q microresonator, Opt. Express **21**, 5988 (2013).

[71] C. Liu, M. V. Gurudev Dutt, and D. Pekker, Single-photon heralded two-qubit unitary gates for pairs of nitrogen-vacancy centers in diamond, Phys. Rev. A **98**, 052342 (2018).

[72] H.-R. Wei and F.-G. Deng, Compact quantum gates on electron-spin qubits assisted by diamond nitrogen-vacancy centers inside cavities, Phys. Rev. A **88**, 042323 (2013).

[73] T.-J. Wang and C. Wang, Universal hybrid three-qubit quantum gates assisted by a nitrogen-vacancy center coupled with a whispering-gallery-mode microresonator, Phys. Rev. A **90**, 052310 (2014).

[74] B.-C. Ren, G.-Y. Wang, and F.-G. Deng, Universal hyperparallel hybrid photonic quantum gates with dipole-induced transparency in the weak-coupling regime, Phys. Rev. A **91**, 032328 (2015).

[75] M. Li and M. Zhang, Robust universal photonic quantum gates operable with imperfect processes involved in diamond nitrogen-vacancy centers inside low-Q single-sided cavities, Opt. Express **26**, 33129 (2018).

[76] C. Cao, Y.-W. Duan, X. Chen, R. Zhang, T.-J. Wang, and C. Wang, Implementation of single-photon quantum routing and decoupling using a nitrogen-vacancy center and a whispering-gallery-mode resonator-waveguide system, Opt. Express **25**, 16931 (2017).

[77] K. Nemoto, M. Trupke, S. J. Devitt, A. M. Stephens, B. Scharfenberger, K. Buczak, T. Nöbauer, M. S. Everitt, J. Schmiedmayer, and W. J. Munro, Photonic Architecture for Scalable Quantum Information Processing in Diamond, Phys. Rev. X **4**, 031022 (2014).

[78] D. Buterakos, E. Barnes, and S. E. Economou, Deterministic Generation of All-Photonic Quantum Repeaters from Solid-State Emitters, Phys. Rev. X **7**, 041023 (2017).

[79] J. Borregaard, H. Pichler, T. Schröder, M. D. Lukin, P. Lodahl, and A. S. Sørensen, One-Way Quantum Repeater Based on Near-Deterministic Photon-Emitter Interfaces, Phys. Rev. X **10**, 021071 (2020).

[80] N. Lo Piparo, M. Razavi, and W. J. Munro, Measurement-device-independent quantum key distribution with nitrogen vacancy centers in diamond, Phys. Rev. A **95**, 022338 (2017).

[81] N. Lo Piparo, M. Razavi, and W. J. Munro, Memory-assisted quantum key distribution with a single nitrogen-vacancy center, Phys. Rev. A **96**, 052313 (2017).

[82] R. E. Evans, M. K. Bhaskar, D. D. Sukachev, C. T. Nguyen, A. Sipahigil, M. J. Burek, B. Machielse, G. H. Zhang, A. S. Zibrov, E. Bielejec, H. Park, M. Lončar, and M. D. Lukin, Photon-mediated interactions between quantum emitters in a diamond nanocavity, Science **362**, 662 (2018).

[83] C. T. Nguyen, D. D. Sukachev, M. K. Bhaskar, B. Machielse, D. S. Levonian, E. N. Knall, P. Stroganov, R. Riedinger, H. Park, M. Lončar, and M. D. Lukin, Quantum Network Nodes Based on Diamond Qubits with an Efficient Nanophotonic Interface, Phys. Rev. Lett. **123**, 183602 (2019).

[84] M. K. Bhaskar, R. Riedinger, B. Machielse, D. S. Levonian, C. T. Nguyen, E. N. Knall, H. Park, D. Englund, M. Lončar, D. D. Sukachev, and M. D. Lukin, Experimental demonstration of memory-enhanced quantum communication, Nature (London) **580**, 60 (2020).

[85] B. Li, P.-B. Li, Y. Zhou, S.-L. Ma, and F.-L. Li, Quantum microwave-optical interface with nitrogen-vacancy centers in diamond, Phys. Rev. A **96**, 032342 (2017).

[86] C.-H. Li and P.-B. Li, Coupling a single nitrogen-vacancy center with a superconducting qubit via the electro-optic effect, Phys. Rev. A **97**, 052319 (2018).

[87] M. Pompili, S. L. N. Hermans, S. Baier, H. K. C. Beukers, P. C. Humphreys, R. N. Schouten, R. F. L. Vermeulen, M. J. Tiggelman, L. dos Santos Martins, B. Dirkse, S. Wehner, and R. Hanson, Realization of a multinode quantum network of remote solid-state qubits, Science **372**, 259 (2021).

[88] Y. F. Pu, N. Jiang, W. Chang, H. Yang, C. Li, and L. M. Duan, Experimental realization of a multiplexed quantum memory with 225 individually accessible memory cells, Nat. Commun. **8**, 15359 (2017).

[89] C. Li, Y.-K. Wu, W. Chang, S. Zhang, Y.-F. Pu, N. Jiang, and L.-M. Duan, High-dimensional entanglement between a photon and a multiplexed atomic quantum memory, Phys. Rev. A **101**, 032312 (2020).

[90] N. Lo Piparo, M. Hanks, C. Gravel, K. Nemoto, and W. J. Munro, Resource Reduction for Distributed Quantum Information Processing using Quantum Multiplexed Photons, Phys. Rev. Lett. **124**, 210503 (2020).

[91] P. Dhara, N. M. Linke, E. Waks, S. Guha, and K. P. Seshadreesan, Multiplexed quantum repeaters based on dual-species trapped-ion systems, arXiv:2105.06707.

[92] Z. Qi, Y. Li, Y. Huang, J. Feng, Y. Zheng, and X. Chen, A 15-user quantum secure direct communication network, Light Sci. Appl. **10**, 183 (2021).

[93] S. Wengerowsky, S. K. Joshi, F. Steinlechner, H. Hübel, and R. Ursin, An entanglement-based wavelength-multiplexed quantum communication network, Nature (London) **564**, 225 (2018).

[94] M. W. Doherty, N. B. Manson, P. Delaney, F. Jelezko, J. Wrachtrup, and L. C. Hollenberg, The nitrogen-vacancy colour centre in diamond, Phys. Rep. **528**, 1 (2013).

[95] M. Hanks, M. Trupke, J. Schmiedmayer, W. J. Munro, and K. Nemoto, High-fidelity spin measurement on the nitrogen-vacancy center, New J. Phys. **19**, 103002 (2017).

[96] F. Kalhor, L.-P. Yang, L. Bauer, and Z. Jacob, Quantum sensing of photonic spin density using a single spin qubit, Phys. Rev. Research **3**, 043007 (2021).

[97] E. Waks and J. Vuckovic, Dispersive properties and large kerr nonlinearities using dipole-induced transparency in a single-sided cavity, Phys. Rev. A **73**, 041803(R) (2006).

[98] M. Ruf, N. H. Wan, H. Choi, D. Englund, and R. Hanson, Quantum networks based on color centers in diamond, J. Appl. Phys. **130**, 070901 (2021).

[99] P. Lodahl, S. Mahmoodian, and S. Stobbe, Interfacing single photons and single quantum dots with photonic nanostructures, Rev. Mod. Phys. **87**, 347 (2015).

[100] M. J. Burek, C. Meuwly, R. E. Evans, M. K. Bhaskar, A. Sipahigil, S. Meesala, B. Machielse, D. D. Sukachev, C. T. Nguyen, J. L. Pacheco, E. Bielejec, M. D. Lukin, and M. Lončar, Fiber-Coupled Diamond Quantum Nanophotonic Interface, Phys. Rev. Appl. **8**, 024026 (2017).

[101] G. T. Reed, G. Mashanovich, F. Y. Gardes, and D. J. Thomson, Silicon optical modulators, Nat. Photon. **4**, 518 (2010).

[102] C. Wang, M. Zhang, X. Chen, M. Bertrand, A. Shams-Ansari, S. Chandrasekhar, P. Winzer, and M. Lončar, Integrated lithium niobate electro-optic modulators operating at cmos-compatible voltages, Nature (London) **562**, 101 (2018).